Article

Hierarchical Composite Membranes with Robust Omniphobic Surface Using Layer-By-Layer Assembly Technique

Yun Chul Woo, Youngjin Kim, Minwei Yao, Leonard Demegilio Tijing, Juneseok Choi, Sangho Lee, Seunghyun Kim, and Hokyong Shon

Environ. Sci. Technol., **Just Accepted Manuscript** • DOI: 10.1021/acs.est.7b05450 • Publication Date (Web): 16 Jan 2018

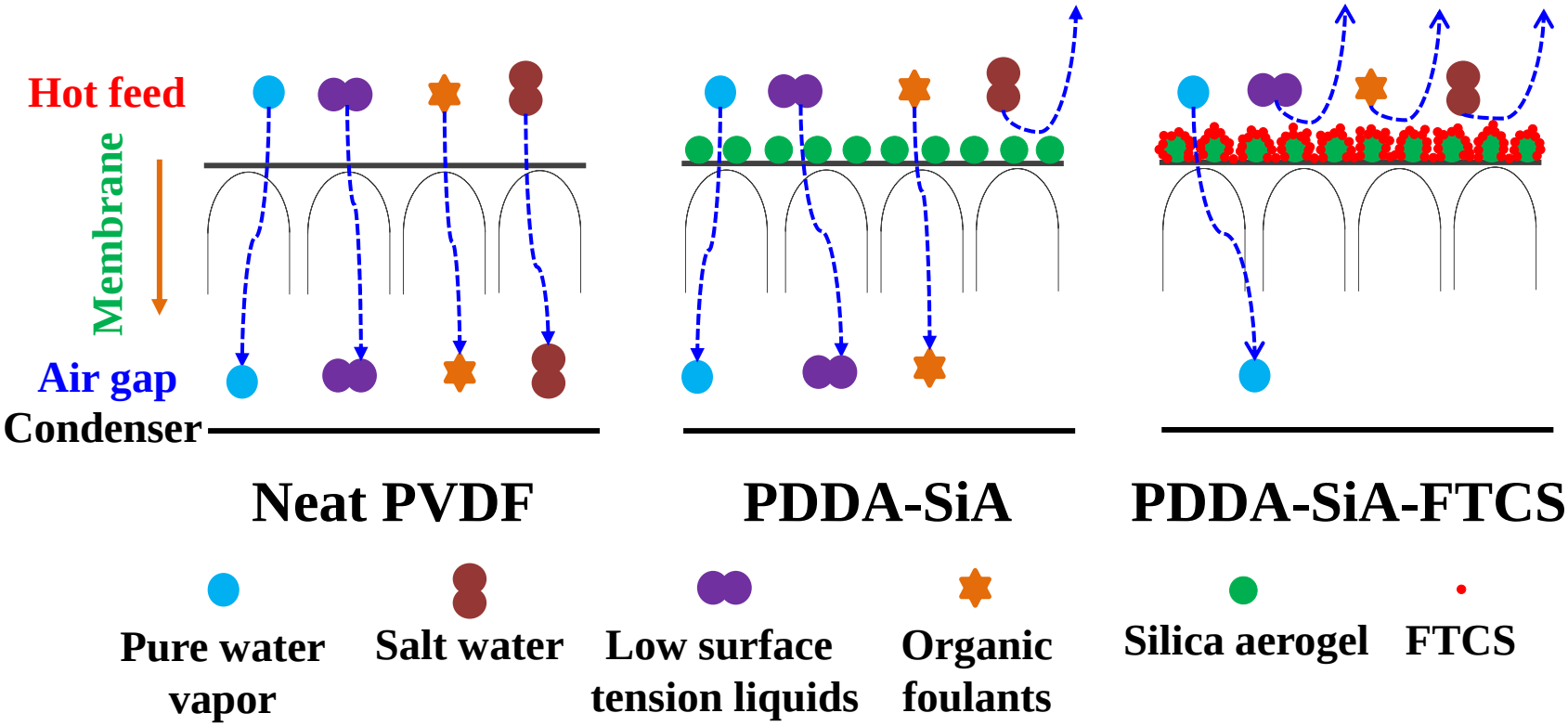
Hot feed
Membrane
Air gap
Condenser
Neat PVDF
PDDA-SiA
PDDA-SiA-FTCS
Pure water vapor
Salt water
Low surface tension liquids
Organic foulants
Silica aerogel
FTCS

Hierarchical Composite Membranes with Robust Omniphobic Surface Using Layer-By-Layer Assembly Technique

Yun Chul Woo[†], Youngjin Kim[‡], Minwei Yao[†], Leonard D. Tijing[†,], June-Seok Choi[§], Sangho Lee[∥], Seung-Hyun Kim[⊥], Ho Kyong Shon[†,*]*

[†]Centre for Technology in Water and Wastewater, School of Civil and Environmental Engineering, University of Technology Sydney (UTS) P. O. Box 123, 15 Broadway, NSW 2007, Australia

[‡]King Abdullah University of Science and Technology (KAUST), Water Desalination and Reuse Center (WDRC), Division of Biological & Environmental Science & Engineering (BESE), Thuwal 23955-6900, Saudi Arabia

[§]Environment and Plant Research Institute, Korea Institute of Civil Engineering and Building Technology (KICT), 283, Goyangdae-Ro, Ilsanseo-Gu, Goyang-Si, Gyeonggi-Do 411-712, Republic of Korea

[∥]School of Civil and Environmental Engineering, Kookmin University, 77 Jeongneung-ro, Jung-gu, Seoul, 136-702, Republic of Korea

[⊥]Department of Civil Engineering, Kyungnam University, Wolyoung-dong, Changwon 631-701, Republic of Korea

KEYWORDS: Membrane distillation, omniphobic, layer-by-layer, surface modification, hierarchical structure.

ABSTRACT

In this study, composite membranes were fabricated via layer-by-layer (LBL) assembly of negatively-charged silica aerogel (SiA) and 1H, 1H, 2H, 2H – Perfluorodecyltriethoxysilane (FTCS) on a polyvinylidene fluoride phase inversion membrane, and interconnecting them with positively-charged poly(diallyldimethylammonium chloride) (PDDA) via electrostatic interaction. The results showed that the PDDA-SiA-FTCS coated membrane had significantly enhanced the membrane structure and properties. New trifluoromethyl and tetrafluoroethylene bonds appeared at the surface of the coated membrane, which led to lower surface free energy of the composite membrane. Additionally, the LBL membrane showed increased surface roughness. The improved structure and property gave the LBL membrane an omniphobic property, as indicated by its good wetting resistance. The membrane performed a stable air gap membrane distillation (AGMD) flux of 11.22 L/m^{2}h with very high salt rejection using reverse osmosis brine from coal seam gas produced water as feed with the addition of up to 0.5 mM SDS solution. This performance was much better compared to those of the neat membrane. The present study suggests that the enhanced membrane properties with good omniphobicity *via* LBL assembly make the porous membranes suitable for long-term AGMD operation with stable permeation flux when treating challenging saline wastewater containing low surface tension organic contaminants.

INTRODUCTION

Membrane distillation (MD) is a thermally-driven membrane separation process that is suitable to treat highly saline waters such as seawater, reverse osmosis (RO) brine, and shale and coal seam gas (CSG, or coal bed methane) produced waters.[1-5] Driving force of MD is the vapor pressure gradient between hot feed water and cold permeate water, so unlike RO, negligible external pressure is applied on the membranes.[6] Therefore, a compact MD system with membranes made of non-corrosive and cheap plastic materials is feasible due to low hydraulic pressure. So far, MD presents a very promising prospect for portable and stand-alone desalination and mining processes.[7] Even though MD has lots of advantages compared with other processes, the technology has still not been carried out into the industrial level because of the lack of an ideally-designed membrane against membrane fouling and wetting issues.[6, 8] Organic and inorganic foulants adhere on the membrane surface during MD operation and they eventually block the pores, which can reduce water flux performance. Membrane wetting is the most critical issue in MD as it can greatly reduce the flux performance and permeate quality. Only vapor is supposed to pass through the membrane to produce pure water in MD. However, liquid water from feed solution may penetrate the membranes, leading to membrane wetting problem. Commonly, some hydrophobic microfiltration (MF) membranes have been utilized in the MD studies, but they still have wetting issues with sub-optimal permeation performance. Hence, there is a need to develop adequate and robust membranes for MD process.[9]

To prevent wetting issues while maintaining adequate water vapor flux performance, MD membranes ideally need high porosity, adequate pore size with narrow pore size distribution, high hydrophobicity, and high liquid entry pressure (LEP). Phase inversion is a commonly-used technique for the fabrication of polymer membranes with high performance in MD process.

Nevertheless, phase inversion membranes still suffer from low hydrophobicity, small porosity, and small pore size,[9] which consequently affect the membrane permeability. Recently, surface modification techniques have been carried out to improve the membrane properties.[10, 11] Although the various modification techniques succeeded in improving MD performance to some extent, these modified membranes still suffer from wetting issues. In addition, when treating challenging sources such as shale and CSG produced waters which contain several types of low surface tension organic compounds such as oil and surfactants, more severe membrane wetting issues can occur in phase inversion membranes.[12]

To address the wetting issues, the membrane surface is ideally designed to have omniphobic property, which provides anti-wetting capability for membranes against wastewater containing low surface tension organics like oil and surfactants. Hence, the MD process can be particularly attractive for the treatment of challenging waters such as textile and dye wastewaters, shale gas produced water and CSG produced water.[1, 2, 13] Omniphobic means: "omni = all" and "phobic = repelling".[14, 15] Therefore, omniphobic membranes exposed to air are supposed to repel all liquids including low surface tension liquids such as oil. The main reason why omniphobicity contributed by membrane surface modification is preferred is that it maintains the highly porous structure of the base polymer membrane while creating multi-layered structure with relatively rough surface. Creating hierarchical structure is one of the major ways to achieve omniphobicity on the membrane surface by surface modification. As numerous air pockets are trapped on the membrane surface, the adhesive force between liquids and the membrane surface can be reduced significantly on the hierarchical structure.[16-18] Among the many modification techniques, the layer-by-layer (LBL) assembly technique is one of the

simplest to create hierarchical structure on the membrane surface, with good potential for scalability.[19-22] This technique is relatively cost-effective and is environment-friendly.[23]

In the present study, we fabricated an omniphobic membrane with strong wetting resistance even to challenging wastewaters by conducting LBL assembly on the fabricated PVDF phase-inversion membrane. A step-by-step dip coating method was applied on the phase inversion membrane to provide LBL assembly. A comparative study was carried out to determine the most important factor in LBL approach. The LBL-modified membranes were examined by physical and chemical characterization to confirm omniphobicity on the membrane surface. The flux and wetting resistance performance of the modified membrane was evaluated in an air gap MD (AGMD) experiment with real RO brine from CSG produced water as feed, and the performance was compared to that of neat PVDF membrane.

EXPERIMENTAL METHODS

- **Materials**

Poly(vinylidene fluoride) (PVDF, Kynar® 761, Mw = 441,000 g/mol) was purchased from Arkema Inc., Australia. N, N-dimethylformamide (DMF), sodium dodecyl sulfate (SDS), ethylene glycol, methanol, 1H, 1H, 2H, 2H – Perfluorodecyltriethoxysilane (FTCS), poly(diallyldimethylammonium chloride) (PDDA, average Mw < 100,000 g/mol, 35 wt% in H_2O) solution, humic acid, and lithium chloride (LiCl) were all purchased from Sigma-Aldrich, Australia. Silica aerogel powder (referred herein as SiA, JIOS AeroVa® powder) was purchased from JIOS, South Korea. SiA has a pore diameter of less than 20 nm, particle size range of 1 ~ 20 μm, and surface area of 600 ~ 1,000 m^2/g according to the information provided by the

manufacturer. All chemicals were used as received. Deionized (DI) water from a Millipore Milli-Q water system was also used.

- **Membrane fabrication**

The neat PVDF phase inversion membrane was prepared following similar fabrication protocol reported in our previous study.[24] Briefly, PVDF of 7 wt% was first dispersed in a certain amount of DMF (90 wt%). After that, the solution was mixed with 3 wt% LiCl by stirring (200 rpm) at 80°C for 2 h. Then, the PVDF solution was further stirred (120 rpm) at 30°C for at least 24 h. To fabricate PVDF flat-sheet membrane, the PVDF solution was poured over a glass plate and was gently lathered by a casting knife at a gap of 300 μm. Then, the lathered film solution was immediately immersed into a coagulation bath (de-ionized water, DI water) for 1 h. After completing coagulation, the membrane was transferred and immersed into another coagulation bath (DI water) for 24 h to remove the residual solvents, and afterwards, it was rinsed with DI water, followed by drying in air at room temperature until a dry flat-sheet membrane was obtained.[24]

- **Surface modification by PDDA-SiA-FTCS**

The layer-by-layer (LBL) surface modification procedure is illustrated in **Figure 1**. The hierarchical composite surface structure composed of PDDA, SiA and FTCS (PDDA-SiA-FTCS) was created on the membrane surface via LBL dip-coating procedure. The fabricated PVDF membrane was used as the base membrane, which was fixed on an acrylic plate by clipping acrylic frame on top of the membrane surface. The LBL surface modification took six steps: 1) 5 wt% PDDA (positive charge), which is one of the polyelectrolytes, was mixed with DI water by stirring for 2 h. After that, the PDDA solution was poured on to the PVDF membrane surface and kept in dry-oven at 60°C for 40 min to form a uniform PDDA layer onto the PVDF

membrane surface, and then, the PDDA coated PVDF was rinsed with DI water to remove residual PDDA solution and dried by nitrogen (N_2) gas (**Fig. 1(a)**); 2) 5 wt% SiA (negative charge) was dispersed in ethanol by sonication for 3 h. Then the SiA solution was poured on to the PDDA coated PVDF membrane surface and kept in dry-oven at 60°C for 1 h. After that the SiA coated PDDA-PVDF membrane was rinsed with DI water and dried by N_2 gas (**Fig. 1(b)**); 3) Then, additional layer of 5 wt% SiA was applied following the same process in step 2 (**Fig. 1(c)**); 4) The fluorination step follows to generate the omniphobic property onto the membrane surface. To do this, 5 wt% FTCS was dissolved in ethanol by stirring for 1 h, and then the FTCS solution was poured on the PDDA-SiA coated PVDF membrane and kept in dry-oven at 60°C for 2 h. After that the FTCS coated PDDA-SiA-PVDF membrane was rinsed with DI water and dried by N_2 gas (**Fig. 1(d)**); 5) The PDDA-SiA-FTCS coated PVDF membrane was kept in dry-oven at 60°C for 24 h.

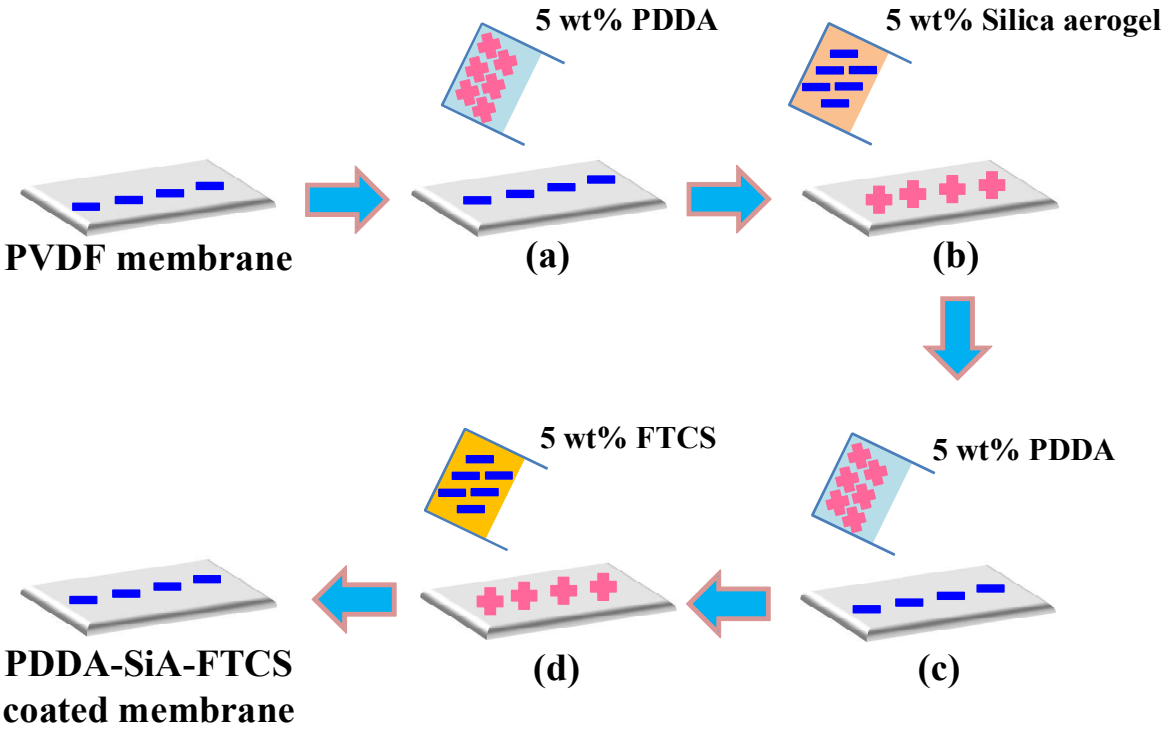

Figure 1 Graphical illustration for the surface modification of the PDDA-SiA-FTCS by layer-by-layer (LBL) assembly technique via electrostatic interaction: (a) the PDDA solution was poured on to the neat PVDF membrane, (b) 5 wt% SiA was applied on the PDDA coated membrane (membrane code is PDDA-SiA), (c) the PDDA solution was poured on to the PDDA-SiA coated membrane and (d) 5 wt% FTCS was poured on to the PDDA-SiA-PDDA coated membrane.

- **Air gap membrane distillation (AGMD) set-up**

The AGMD set-up for performance test was the same as the one in our previous work.[25] The membranes were tested in a home-made AGMD set-up with an effective membrane area of 21 cm^2 and a feed channel dimension of 60 mm × 35 mm × 1 mm (L × W × H). The thickness of the air gap was 3 mm. The coolant plate was made of a stainless steel (SUS-316L) to condense the water vapor and produce pure water. The AGMD in a co-current flow set-up was carried out

158 with constant inlet temperatures at the feed and the coolant sides of 60.0 ± 1.5°C and 20.0 ±
159 1.5°C, respectively. The feed solution was real RO brine from CSG produced water (from
160 Gloucester Basin located along the lower north coast of New South Wales, Australia) with
161 conductivity of around 22.6 mS/cm and the coolant fluid was tap water.[13, 26] The feed and
162 coolant circulation rates were both maintained at 24 L/h.

163 ▪ **Membrane characterizations**

164 The membrane porosity, defined as the volume of pores divided by the total volume of
165 the membrane, was measured via a gravimetric method.[7] The pore size of the neat and LBL
166 assembled phase inversion membranes was measured by capillary flow porometry (CFP-1200-
167 AEXL). All samples were firstly applied with N_2 gas to determine the gas permeability.[7]
168 Galwick (surface tension of 15.9 mN/m) was used in both the porosity and capillary flow
169 porometry measurements to wet the membrane. The surface morphology of the fabricated and
170 LBL assembled membranes was observed by scanning electron microscopy (SEM, Zeiss Supra
171 55VP, Carl Zeiss AG). Membrane surface roughness was analyzed by atomic force microscopy
172 (AFM) imaging. AFM was carried out under ambient conditions in non-contact mode with
173 silicon probes (Dimension 3100 Scanning Probe Microscope, Bruker).[24] Zeta potential of the
174 membrane was examined by a streaming current electro-kinetic analyzer (SurPass, Anton Paar
175 GmbH, Austria).[27-29] The mechanical properties of the different membrane samples were
176 measured using a Universal Testing Machine (UTM LS, Lloyd) equipped with a 1 kN load cell.
177 Thermogravimetric analysis (TGA) was carried out using a Q600 (TA Instuments). The
178 fabricated membranes were heated to 800°C at a rate of 10°C/min in N_2. The fabricated and LBL
179 assembled membranes were measured by X-ray photoelectron spectroscopy (ESCALAB250Xi,
180 Thermo Scientific, UK) with a monochromated Al K alpha X-ray source (1486.68 eV), and the

pressure in the analyzing vacuum chamber was higher than 2×10^{-9} mbar. Surface survey data was obtained by high resolution scans. Peak areas and relative peak area ratios were calculated by software (Avantage).

- **Contact angle (CA) and sliding angle (SA)**

In order to compare the wettability and omniphobic properties of neat and modified membranes, surface contact angle (CA) was measured. The CA of the membranes was measured using the sessile drop method with an optical subsystem (Theta Lite 100) integrated with image-processing software. Membrane samples were placed on a flat platform and 5 µL droplets of water (Surface tension, γ = 72.80 mN/m), methanol (γ= 22.70 mN/m), mineral oil ($\gamma \approx$ 30.0 mN/m), and ethylene glycol (γ = 47.70 mN/m) were dropped carefully on the membrane surface.[30] The wettability of a membrane surface can be expressed in terms of the contact angle (θ), which is governed by Young's equation as follows:[30]

$$\gamma_m = \gamma_{ml} + \gamma_l \cos\theta \qquad \textbf{(Eq. 1)}$$

where, γ_m, γ_{ml}, and γ_l represent the surface tensions of membrane in contact with air, membrane in contact with liquid, and liquid in contact with air, respectively.

Water sliding angle (SA) is one of the significant properties for MD, and a small angle is expected for high hydrophobicity. SA shows the difference between advancing and receding CA, i.e., hysteresis.[31, 32] A 10 µL water droplet was first horizontally placed on membranes. The droplet was then gradually tilted until it started to slide on the membrane surface, and that tilting angle was recorded as SA.[33]

RESULTS AND DISCUSSION

- **Surface zeta potential of the neat PVDF and LBL modified membranes**

Figure 2 illustrates the surface zeta potentials of the neat PVDF, PDDA-SiA, and PDDA-SiA-FTCS assembled membranes as a function of pH. The PDDA-SiA-FTCS assembled membrane showed a decreased charge on the surface compared with the neat PVDF membrane due to the presence of negatively-charged FTCS on the membrane surface.[34] The isoelectric point (point of zero charge) of the PDDA-SiA-FTCS assembled membrane was below 4.2, while those of neat PVDF and PDDA-SiA assembled membranes were <5.9 and <5.5, respectively. A more negatively-charged PDDA-SiA-FTCS assembled membrane can potentially better mitigate fouling problems against natural organic matters (NOM) such as humic and fulvic acids compared with the neat PVDF and PDDA-SiA assembled membrane.[35]

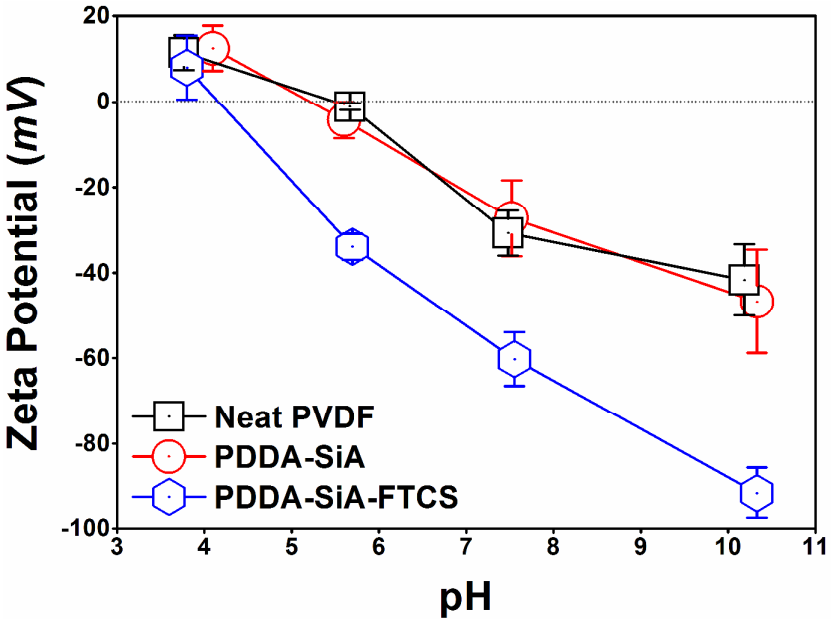

Figure 2 Zeta potentials of the neat PVDF phase inverted membrane, the PDDA-SiA, and PDDA-SiA-FTCS assembled membranes. The background electrolyte concentration is 0.01 M KCl. Solution pH varies from 4 to 10.

- **Effects of LBL coating on the membrane surface**

The SEM images showing the surface morphology of the neat PVDF membrane, PDDA-SiA, and PDDA-SiA-FTCS assembled membrane are presented in **Fig. 3(a – c)**. In **Fig. 3(a)**, the neat PVDF membrane has smooth surface with slightly open pore structure. LBL assembly technique is one of the effective approaches to create dense active layers onto the membrane.[36] The PDDA-SiA assembled membrane shows partial dense layers with particle-like features on the membrane surface, which means that it is not assembled well (**Fig. 3(b)**). On the other hand, the surface-active layer of the PDDA-SiA-FTCS assembled membrane seems to be much denser than the surfaces of other membranes and exhibits rough and particle-like features (**Fig. 3(c)**). Based on the observation of the SEM images, the PDDA-SiA-FTCS was more successfully modified on to the neat PVDF membrane by LBL assembly technique than on the PDDA-SiA membrane. The cross-sectional SEM image of the PDDA-SiA-FTCS membrane shows that LBL layers well adhered on the PVDF membrane surface, while the PDDA-SiA membrane did not adhere well (**Fig. S1(a – c)**).

Fig. 3(d – f) shows the images of water droplet movement on the membrane surface, providing evidence of the hydrophobicity of each membrane. A small contact angle can be observed when the water droplet is dropped onto the neat PVDF membrane surface, which shows a low hydrophobicity (**Fig. 3(g)**). Meanwhile, PDDA-SiA assembled membrane obtained much higher hydrophobicity reaching superhydrophobicity (CA of 154.1°), PDDA-SiA-FTCS assembled membrane also obtained superhydrophobic surface (>170^{o}) (**Fig. 3(f)**), with an interesting observation of a lotus effect, i.e., the water droplet is sliding away on the membrane surface (sliding angle was only 1.1 ± 0.3°), mainly attributed to both the very low surface free energy and high surface nano-roughness of the membrane. In comparison, the SA of PDDA-SiA

241 membrane was 34.3 ± 1.6°, while neat PVDF membrane was showing petal effect, i.e., water
242 droplet adheres on the membrane at any angle. These results indicate the potential of both the
243 PDDA-SiA and the PDDA-SiA-FTCS assembled membranes in mitigating membrane wetting
244 problems during MD operation due to their superhydrophobicity and near lotus effect.

245 To check whether the membranes have omniphobic properties, several low surface
246 tension liquids such as ethylene glycol (γ = 47.70 mN/m), mineral oil ($\gamma \approx$ 30.0 mN/m) and
247 methanol (γ= 22.70 mN/m) were dropped on to the surface of the modified membranes for CA
248 measurement (see **Fig. 3(h)**). The neat PVDF membrane showed low hydrophobicity which is
249 common among the membranes fabricated by non-solvent induced phase separation (NIPS)
250 method.[9] Rapid wicking occurred when the neat membrane was exposed to low surface tension
251 liquids. In addition, wicking problems were also observed on the PDDA-SiA assembled
252 membrane when exposed to mineral oil and methanol, while a bit resistant to ethylene glycol.
253 This is interesting as the PDDA-SiA membrane showed high water hydrophobicity (>150^{o})
254 previously. The relatively high wettability of both neat PVDF and PDDA-SiA assembled
255 membranes is attributed to the relatively high surface energy of PVDF and SiA.[13] On the other
256 hand, the PDDA-SiA-FTCS assembled membrane showed high CAs to water, ethylene glycol,
257 mineral oil and methanol, which indicated good omniphobic property after FTCS assembly. The
258 enhancement in omniphobic property of the assembled membrane is mainly attributed to the
259 successful applied homogenous fluorination on the membrane surface during FTCS assembly,
260 leading to low surface energy of the PDDA-SiA-FTCS assembled membrane. Due to its
261 omniphobic property, the PDDA-SiA-FTCS assembled membrane presents good potential to
262 treat textile, dye and CSG produced water containing low surface tension organic compounds.
263

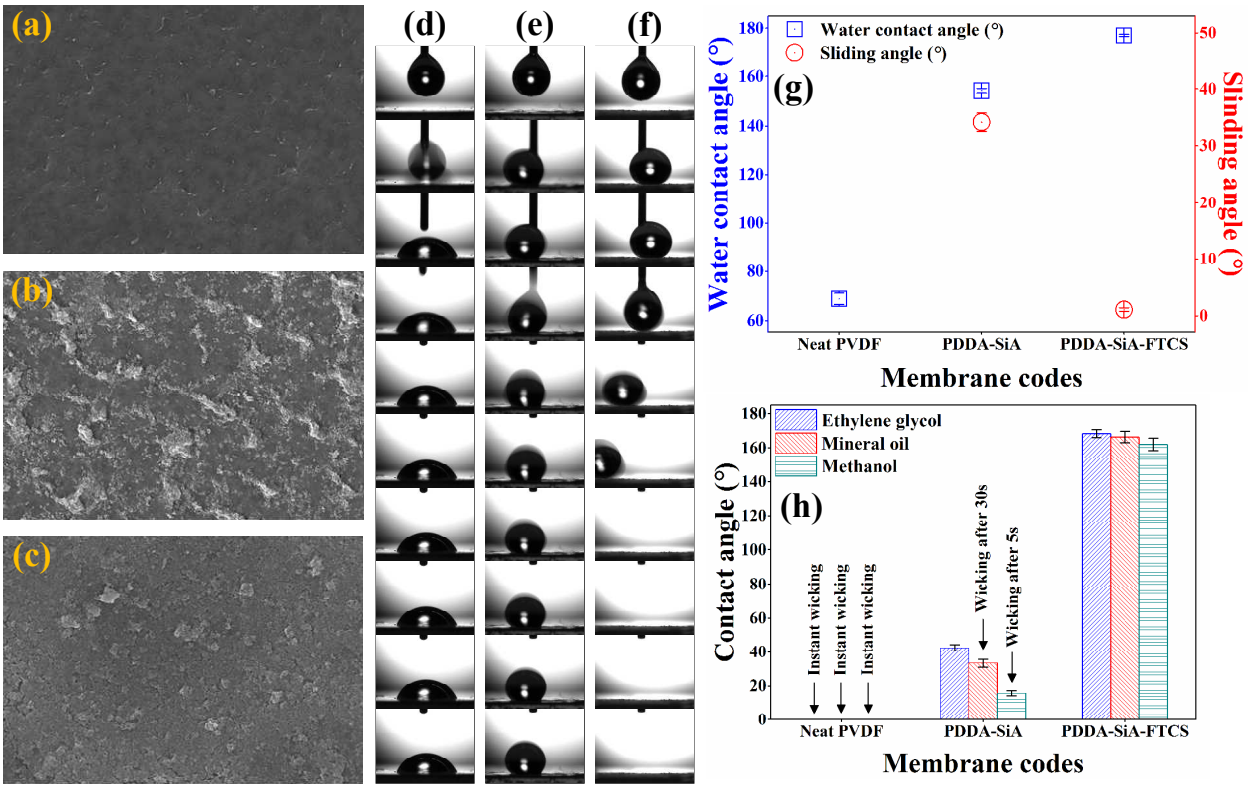

Figure 3 (a, b, c) Surface SEM images of (a) the neat PVDF membrane, (b) PDDA-SiA, and (c) PDDA-SiA-FTCS assembled membranes, (d, e, f) captured images of water droplet movement on the surface of (d) the neat PVDF membrane, (e) PDDA-SiA, and (f) PDDA-SiA-FTCS assembled membranes, (g) water (γ = 72.0 mN/m) contact and sliding angles on the neat PVDF membrane (CA of 68.9 ± 2.3°), PDDA-SiA (CA of 154.1 ± 0.9°), and PDDA-SiA-FTCS (CA of 177.0 ± 0.4°) assembled membranes, (h) contact angles of low surface tension liquids such as ethylene glycol (γ = 47.7 mN/m), mineral oil (γ = 30.0 mN/m), and methanol (γ = 22.7 mN/m) on the neat PVDF membrane, PDDA-SiA, and PDDA-SiA-FTCS assembled membranes.

- **Chemical and physical properties of the membrane surface.**

The surface contact angles of the LBL assembled membranes were improved compared with the neat PVDF membrane. As the surface roughness is the other main contributor to the wetting properties of the membrane, the roughness of the neat and LBL assembled membranes was examined by AFM. It was found that the LBL assembled membranes had much rougher nano-roughness surface compared with those of neat PVDF membrane and PDDA-SiA assembled membrane, which was attributed to the presence of FTCS (**Fig. 4(a – d)**). As shown in **Fig. 4(d – f)**, the neat PVDF membrane seems to have smooth surface and open pore structure. On the other hand, the PDDA-SiA assembled membrane has lots of silica aerogel particles deposited on the membrane surface (**Fig. 4(e)**). The PDDA-SiA-FTCS assembled membrane showed hierarchical structure as small size particles (FTCS) were forming and protruding on larger size particles (silica aerogel). This leads to the existence of more air pockets between the valleys of the nano-roughness, enhancing the hydrophobicity and omniphobicity of the PDDA-SiA-FTCS membrane. Additionally, FTCS particles with SiA particles led to the formation of the re-entrant structure, which contribute to omniphobic property. Hierarchical nanostructure can potentially mitigate fouling and wetting problems against low surface tension liquids.[17]

In **Fig. 5(a – c)**, the XPS survey scan reveals that C and F are the major components on the surfaces of the neat PVDF and LBL assembled membranes. However, atomic percentages of C and F decreased on the surface of the LBL assembled membranes compared with the neat PVDF membrane, while Si and O increased due to the presence of SiA and FTCS (**Table 1**). The ratio of oxygen to silicon on the PDDA-SiA-FTCS assembled membrane remains identical (≈ 2.0) because of the chemical composition of silicon dioxide.

Fig. 5(d – f) indicates that the neat PVDF membrane has carbon atoms in the form of carbon-carbon (C-C/C=C), carbon-hydrogen (C-H), carbon-oxygen (C=O) and vinylidene

298 fluoride (CF_2-CH_2) bonds, while XPS scans on LBL assembled membranes exhibits new carbon
299 atom bond formations such as carbon fluorine (C-F), tetrafluoroethylene (CF_2-CF_2) and
300 trifluoromethyl (CF_3). Mainly, carbon elements on the neat PVDF membrane surface were in the
301 form of CF_2-CH_2 and C-H status, while those on PDDA-SiA-FTCS membrane were changed to
302 C-F, CF_2-CF_2 status, which led to improved hydrophobicity because they had lower surface
303 tension compared with the CF_2-CH_2 and C-H. Additionally, new CF_3 peaks, well-known to have
304 the lowest surface free energy bond, appeared after FTCS LBL assembly modification (the
305 fluorination step) compared with the PDDA-SiA assembled membrane (**Fig. 5(e, f)** and **Table**
306 **1**).[13] Thus, the PDDA-SiA-FTCS assembled membrane had much higher contact angle and lower
307 surface free energy.

308 The PDDA-SiA assembled membrane showed the lowest atomic percentage of F
309 component among all the membrane samples because the SiA layer was covering the membrane
310 surface, while the PDDA-SiA-FTCS assembled membrane showed that atomic percentage of F
311 component slightly increased after fluorination step by FTCS, which formed silicon dioxide
312 combined with CF_3 and CF_2-CF_2. So, the PDDA-SiA-FTCS assembled membrane had a low
313 surface free energy compared to the PDDA-SiA assembled membrane.

314 Hence, both improved physical and chemical properties of the PDDA-SiA-FTCS
315 assembled membranes achieved after modification contributed to enhanced contact angles to
316 water and low surface tension liquids, which led to enriched omniphobicity.

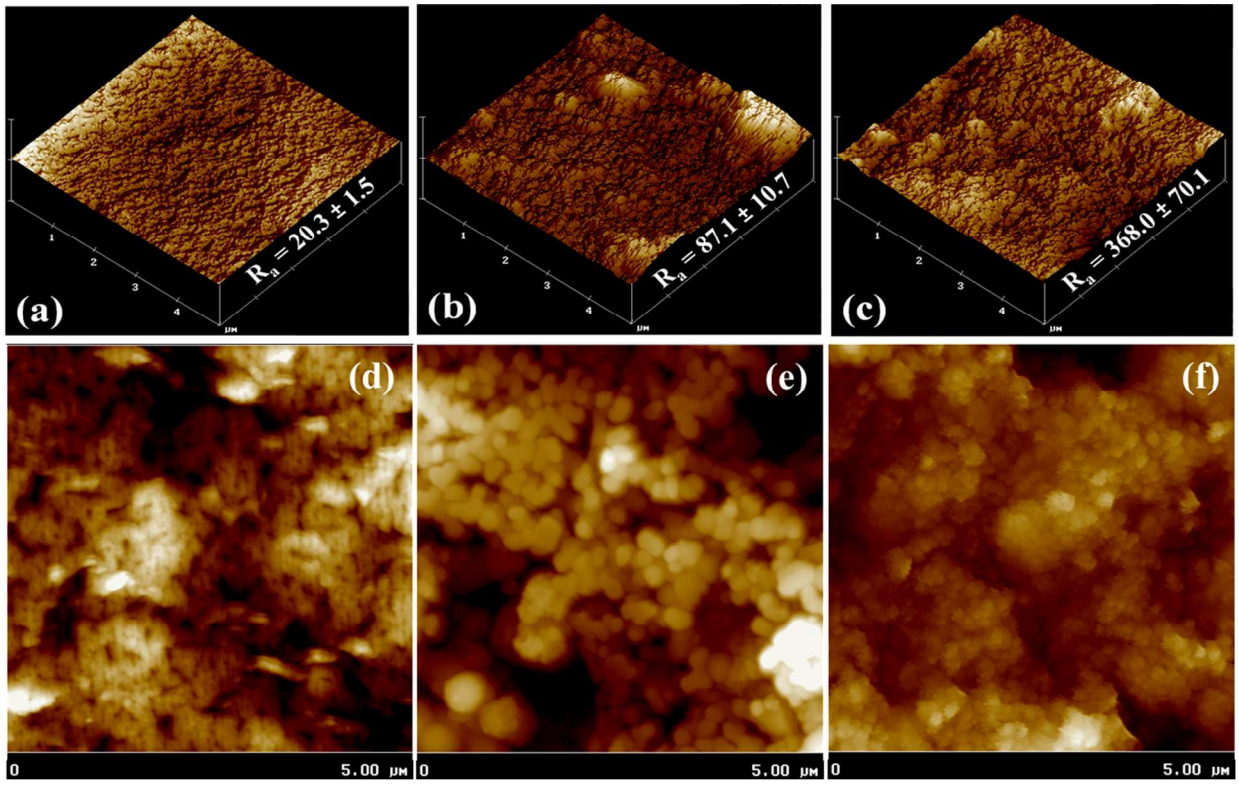

Figure 4 Surface AFM 3D (a – c) and 2D (d – f) images of (a, d) the neat PVDF membrane, (b, e) PDDA-SiA, and (c, f) PDDA-SiA-FTCS assembled membranes. The mean surface roughness (R_a) of the neat PH membrane, PDDA-SiA, and PDDA-SiA-FTCS assembled membranes was 20.3 ± 1.5 nm, 87.1 ± 10.7 nm, and 368.0 ± 70.1 nm, respectively.

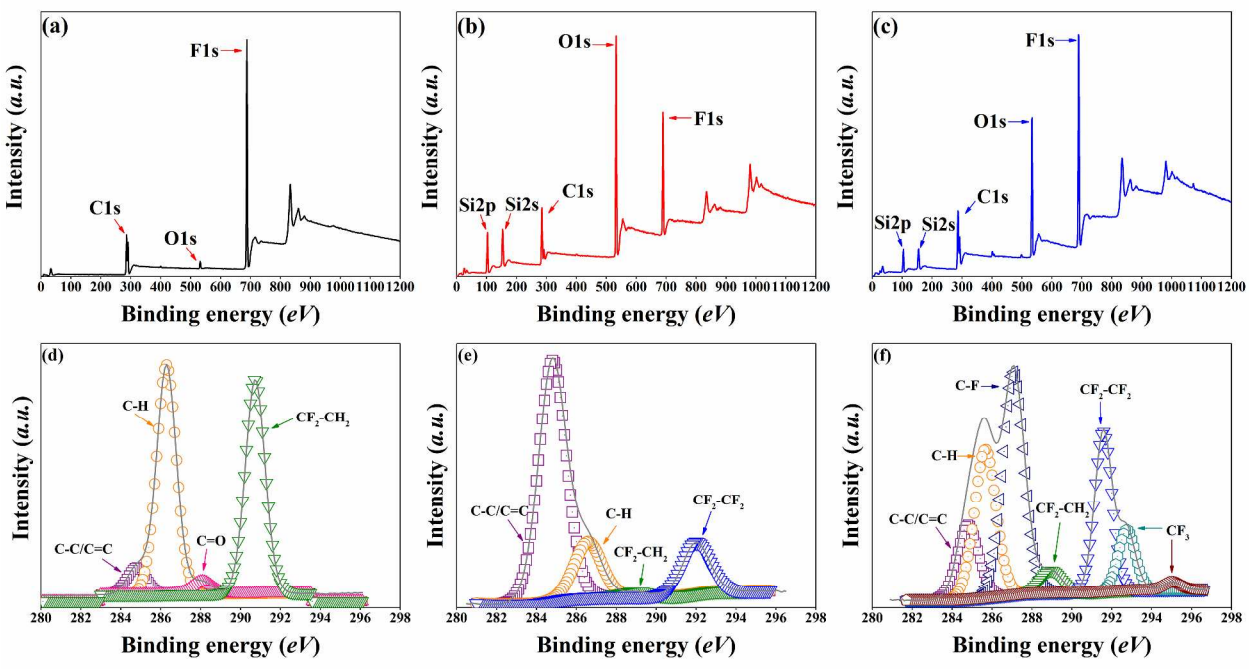

322

323 **Figure 5** Surface XPS (a – c) survey scans and (d – f) carbon spectra of (a, d) the neat PVDF
324 membrane, (b, e) PDDA-SiA, and (c, f) PDDA-SiA-FTCS assembled membranes. Surface
325 survey data was obtained by high resolution scans over C1s (281 - 298 eV), O1s (528 - 540 eV),
326 Cl2p (196 - 208 eV), Si2p (99 - 108 eV), Si2s (144 – 161 eV), and F1s (682 - 695 eV). C1s
327 spectra showed carbon atoms in the form of C-C/C=C (284.80 eV), C-H (286.29 eV), C=O
328 (288.08 eV), and CF_2-CH_2 (288.95 eV) bonds and LBL assembled membranes showed C-F
329 (287.10 eV), CF_2-CF_2 (291.58 eV) and CF_3 (292.75 and 295.03 eV).

330

Table 1 Surface compositions of the neat and coated membranes (all units are at. %).

Membrane code	C							F	O	Si
	C-C/C=C	C-H	C=O	C-F	CF_2-CH_2	CF_2-CF_2	CF_3			
Neat PVDF	2.91	24.18	1.35	0	22.59	0	0	46.57	1.88	0
PDDA-SiA	20.45	4.69	0	0	0.39	4.29	0	13.74	34.22	21.82
PDDA-SiA-FTCS	4.47	8.91	0	13.37	1.37	7.65	3.29	24.8	22.68	11.20

- **Membrane characteristics**

The characteristics of the neat PVDF and LBL assembled membranes are shown in **Table 2**. The thickness of all membranes revealed thinner thickness than other phase-inversion membrane in literature due to its low PVDF concentration.[9, 24] The thickness of the PDDA-SiA-FTCS assembled membranes increased with the increasing amounts of layers compared with the neat PVDF and PDDA-SiA assembled membrane. The mean and maximum pore sizes of the PDDA-SiA-FTCS assembled membranes showed reversed trend as their thickness. Both the increase in thickness and the decrease in mean pore sizes due to additional assembled layers can possibly lead to decreased water vapor flux performance in MD application. Thus, it is important to control the number of LBL layers to a minimum to make a suitable membrane balancing permeation and rejection performances. The neat PVDF membrane showed highly-porous structure (83.2% porosity) because of the low concentration of the PVDF solution (7 wt%

PVDF) used, while the assembled layers had insignificant effects on the porosities. The PDDA-SiA-FTCS assembled membrane had the lowest porosity among three samples. Nevertheless, it still had higher porosity (~79.4%) compared with the commercial PVDF membrane (only ~70%).[25] For MD, higher porosity is ideal so as to allow more vapor to pass through the voids of the membrane leading to increased water flux.[17]

Liquid entry pressure (LEP), i.e., the minimum pressure needed for water molecule to penetrate the membrane pores, is one of the most important factors to prevent wetting issue during MD operation. The higher the LEP, the better is the resistance of the membrane to wetting. Based on the Laplace equation, the LEP of the membrane is proportional to the contact angle and the inverse of the mean pore size.[16] The LEP tests showed that PDDA-SiA-FTCS assembled membrane obtained the highest LEP in the present study. This was attributed to its lower mean pore size and higher contact angle compared to other fabricated membranes in this study. This gives the PDDA-SiA-FTCS assembled membrane more potential for long term MD operation, giving robustness to the membrane and less wetting propensity.

Table 2 Characteristics of the neat and LBL assembled membranes.

Membrane code	Thickness (µm)	Mean pore size (µm)	Maximum pore size (µm)	Porosity (%)	[a]LEP_w (bar)	[b]LEP_S (bar)
Neat	58.2 ± 0.7	0.20 ± 0.03	0.25 ± 0.04	83.2 ± 1.4	1.85 ± 0.11	0.17 ± 0.02
PDDA-SiA	60.6 ± 0.7	0.17 ± 0.02	0.22 ± 0.04	81.3 ± 2.8	2.03 ± 0.14	0.23 ± 0.01
PDDA-SiA-FTCS	62.4 ± 1.0	0.09 ± 0.01	0.18 ± 0.02	79.4 ± 1.6	2.82 ± 0.13	2.04 ± 0.17

[a]LEP_w : Liquid entry pressure against water; [b]LEP_S : Liquid entry pressure against NaCl of 0.6 M with SDS of 3 mM

- **Mechanical and thermal stability of the neat PVDF and LBL assembled membranes.**

The mechanical and thermal properties of the neat PVDF membrane and LBL assembled membranes were examined by UTM and TGA, respectively. It is well known that when assembled layers have good adhesion on the host polymer, they can lead to load transfer from host polymer to assembled layers, thereby enriching its mechanical and thermal properties.[7] In MD applications, the systems are operating at atmospheric pressure, thus giving membranes lower requirements for mechanical integrity. Nevertheless, adequate mechanical properties are still needed to sustain a stable long-term MD operation.[25]

Fig. 6(a) shows the stress-strain curves of the neat PVDF membrane and LBL assembled membranes. The stress-strain curves of the neat PVDF membrane, PDDA-SiA, and PDDA-SiA-FTCS assembled membranes shared similar trends. All membranes shared a steep increase in stress in the first 5% strain, after that, the stress increased gradually until the failure due to a dense structure of the phase-inversion membrane. However, it can be noticed that PDDA-SiA and PDDA-SiA-FTCS assembled membranes resulted in increased tensile strength and strain, with the latter having the highest tensile strength among the samples tested. This confirms that LBL assembly surface modification technique on the PVDF membrane causes good load transfer from PVDF membrane to assembled layers, leading to enhanced mechanical properties.

TGA measurement of the membrane samples is shown in **Fig. 6(b)**. The neat PVDF membrane exhibited a prominent weight loss at 432°C, which is consistent with the temperature when degradation of PVDF occurred. The PDDA-SiA showed a major fraction of thermal decomposition at approximately 18°C higher temperature, which confirmed the enrichment of its thermal stability. The PDDA-SiA-FTCS assembled membrane had a higher major fraction of

thermal decomposition than the PDDA-SiA assembled membrane, which showed that FTCS was able to further improve the thermal stability of the membranes. The weight loss of the neat PVDF membrane, the PDDA-SiA, and PDDA-SiA-FTCS assembled membranes at 500°C was 18.85%, 28.21% and 54.53%, at 600°C was 8.89%, 21.29% and 52.20%, and at 700°C was 2.86%, 17.13% and 50.42%, respectively. Higher residual mass was observed for the PDDA-SiA-FTCS assembled membrane compared with the neat PVDF membrane and PDDA-SiA assembled membrane, indicating that the FTCS layer by the fluorination modification was able to enhance the thermal properties of the membrane.

According to the TGA results, it is believed that PDDA-SiA-FTCS had enhanced binding stability due to the wrapped fluorosilane layers on the silicon dioxide.[1] Also, the electrostatic interaction between negatively charged SiA and FTCS and the positively charged PDDA can enrich the stability of the membrane.[37] Hence, the LBL assembled membrane properties improved a lot compared with the neat PVDF membrane regarding their thermal and mechanical properties. Moreover, the dominant layer of the membrane changed from the PVDF layer to LBL surface modified layer.

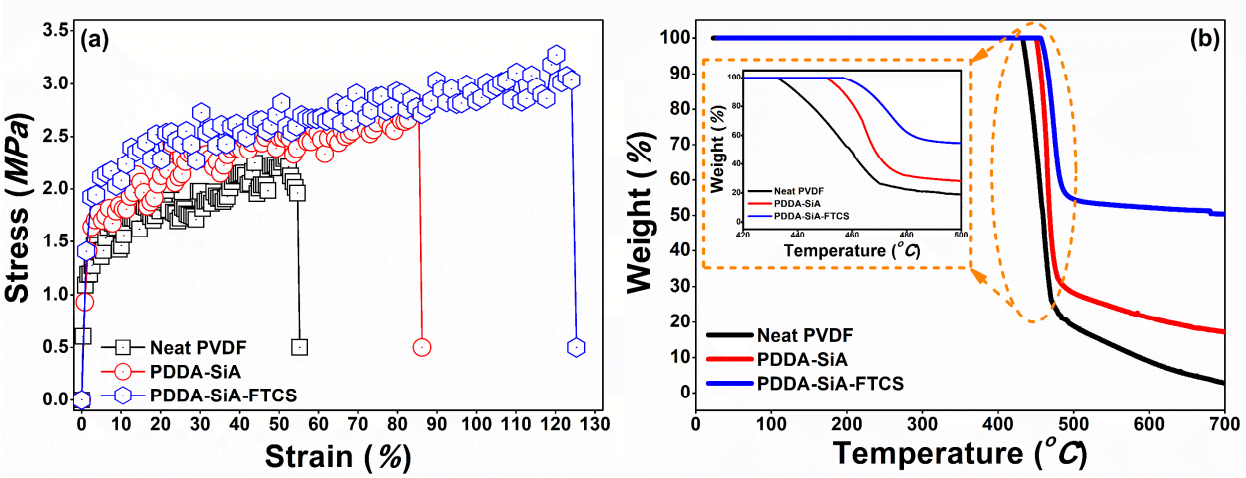

Figure 6 (a) Stress-strain curve and (b) TGA of the neat PVDF membrane, PDDA-SiA, and PDDA-SiA-FTCS assembled membranes. Ultimate tensile strength of the neat PVDF membrane, PDDA-SiA, and PDDA-SiA-FTCS assembled membranes is 2.40 ± 0.08 MPa, 2.78 ± 0.10 MPa, and 3.16 ± 0.16 MPa, respectively, and elongation at break of the neat PVDF membrane, PDDA-SiA, and PDDA-SiA-FTCS assembled membranes is 54.27 ± 3.03%, 85.48 ± 10.99%, and 107.97 ± 14.11%, respectively. In terms of the thermal stability, the major thermal decomposition of the neat PVDF membrane, PDDA-SiA, and PDDA-SiA-FTCS assembled membranes is 432.27°C, 450.21°C, and 456.37°C, respectively.

- **AGMD performance tests using various feed solutions**

The LBL assembled omniphobic membranes in the present study were tested for their performance in the treatment of saline and more challenging (low surface tension liquid and/or organic compound liquid) feed solutions. In the initial part, the flux and salt rejection performance of the neat PVDF and LBL assembled membranes were evaluated for 24 h by AGMD process using real RO brine from CSG produced water as feed. After determining the individual performances of the neat and LBL assembled membranes, the membrane with optimal

418 performance was chosen and further evaluated using a more challenging feed solution which was
419 RO brine from CSG produced water containing different concentrations of surfactants (i.e., SDS)
420 for testing omniphobic properties and organic compounds like humic acid for testing anti-fouling
421 properties.

422 In **Fig. 7(a – c)**, all LBL assembled membranes showed lower flux performance (10.55-
423 11.93 LMH) compared with the neat PVDF membrane (12.89 LMH). The decrease in the water
424 vapor flux for the LBL assembled membranes was likely attributed to the increased thickness
425 due to the deposition layers and hence decreased pore size and porosity **(Table 2)**. Nevertheless,
426 the difference of the flux was insignificant, so the LBL assembled membranes still had an
427 acceptable water vapor flux performance for MD process.

428 Apart from obtaining high water vapor flux, a high salt rejection is also equally if not
429 more important for MD application, so both parameters should be well balanced. Both LBL
430 assembled membranes obtained final permeate salt rejection of almost 100% after 24 h of tests.
431 On the other hand, the neat PVDF membrane had decreased salt rejection performance after 18 h
432 of operations (**Fig. 7(a)**). The fast wetting of the PVDF neat membrane could be due to the
433 presence of some organic contaminants in the RO brine from CSG produced water as these
434 contaminants may penetrate the membrane easily and cause wetting.[24] As observed in **Fig. 3(h)**,
435 the neat PVDF membrane was not able to adequately reject some organic contaminants with low
436 surface tension properties. Even though the LBL assembled membranes could not achieve high
437 water vapor flux performance compared with the neat PVDF membrane, they had much higher
438 salt rejection performance than the neat PVDF membrane. Based on the results, the PDDA-SiA-
439 FTCS membrane showed the optimal performances regarding both flux and salt rejection.

To further evaluate the reliability of the LBL assembled membrane when treating challenging water sources containing surfactants (i.e., SDS) and NOM (i.e., humic acid), respectively. An increasing concentration (from 0.1 to 0.5 mM) of SDS, a common anionic surfactant, was added to the real RO brine from CSG produced water as feed solution (see **Fig. 7(d – f)**). During AGMD operation, SDS was added to the feed every 2 h until a maximum concentration of 0.5 mM was reached. The AGMD performance of the PDDA-SiA-FTCS assembled membrane was compared with those of the neat PVDF membrane and PDDA-SiA assembled membrane. The initial water vapor flux of the PDDA-SiA-FTCS assembled membrane was lower than the other two, which was likely attributed to the smaller pore sizes, lower porosity, and thicker thickness. When adding 0.1 mM SDS after 2 hours of operation, the neat PVDF membrane (**Fig. 7(d)**) showed decreased salt rejection performance and sudden increase in the water vapor flux. Also, the water vapor flux was increased greatly and salt rejection of the PDDA-SiA assembled membrane was decreased when SDS of 0.3 mM was added into the feed water (**Fig. 7(e)**), while the PDDA-SiA-FTCS assembled membrane showed stable flux and salt rejection performances even when the SDS concentration in feed reached 0.5 mM (**Fig. 7(F)**). The surfactant could significantly decrease the surface tension of the feed solution, which can lead to reduction in LEP and hence higher chance of membrane wetting.[12] However, the PDDA-SiA-FTCS assembled membrane still kept a stable normalized water vapor flux and high salt rejection ratio of 100% even after the addition of 0.5 mM of SDS, indicating its high resistance against low surface tension liquid.

Humic acid of 20 mg/L was also added into CSG RO brine as feed to test the anti-fouling properties of the LBL assembled membrane. Results in **Fig. 7(g)-(h)** indicate that, while wetting issues occurred on the neat PVDF (**Fig. 7(g)**) and PDDA-SiA membranes (**Fig. 7(h)**), it did not

463 occur on the PDDA-SiA-FTCS assembled membrane (**Fig. 7 (i)**). The differences of these results
464 are attributed to the changes in zeta potential among the LBL assembled membranes. As shown
465 in **Fig. 2**, zeta potential of the PDDA-SiA-FTCS assembled membrane was higher than those of
466 the neat PVDF and PDDA-SiA membranes, and thus stronger electric-repulsion to humic acid
467 could occur on the PDDA-SiA-FTCS assembled membrane than others, resulting in lower
468 membrane fouling. Therefore, it is believed that the PDDA-SiA-FTCS assembled membrane also
469 had anti-fouling property against organic compounds, and hence was considered having high
470 potential for the treatment of challenging water sources containing low surface tension and
471 organic contaminants. In terms of both flux and salt rejection stability, the PDDA-SiA-FTCS
472 membrane exhibited the optimal performances compared with the neat PVDF and PDDA-SiA
473 assembled membranes. Even though the PDDA-SiA could be a suitable membrane to treat RO
474 brine from CSG produced water by MD process due to its high resistance against wetting, its
475 performance was not acceptable when the feed solution contains low surface tension and/or
476 organic compound liquids.

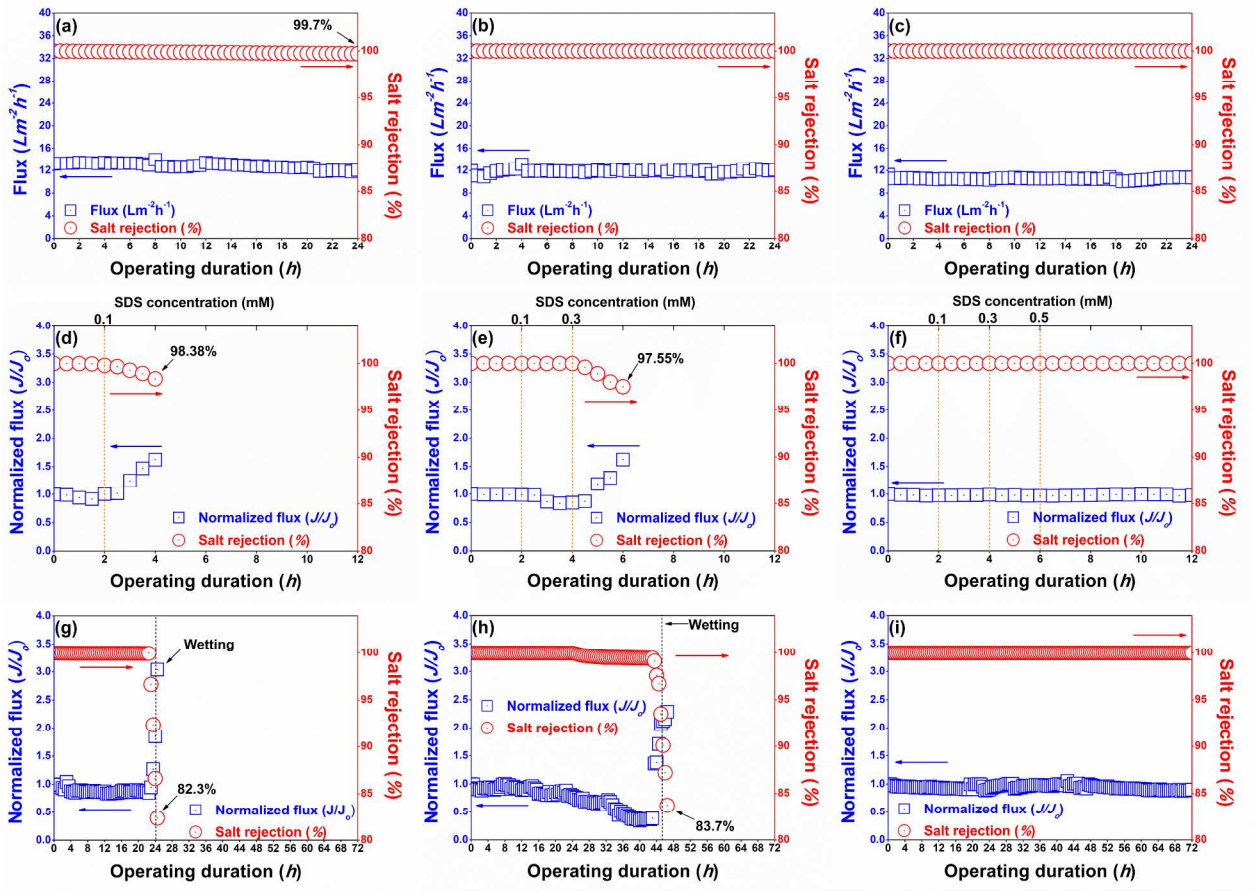

Figure 7 (a, b, c) Water vapor flux and salt rejection performances of (a) the neat PVDF membrane, (b) PDDA-SiA, and (c) PDDA-SiA-FTCS assembled membranes by AGMD process using RO brine from CSG produced water as feed; (d, e, f) normalized water vapor flux and salt rejection performances of (d) the neat PVDF membrane, (e) PDDA-SiA, and (f) PDDA-SiA-FTCS assembled membranes by AGMD process using RO brine from CSG produced water including SDS from 0.1 mM up to 0.5 mM as feed, and; (g, h, i) normalized water vapor flux and salt rejection performances of (g) the neat PVDF membrane, (h) PDDA-SiA, and (i) PDDA-SiA-FTCS assembled membranes by AGMD process using RO brine from CSG produced water including humic acid of 20 mg/L as feed. The initial water vapor flux of the neat, PDDA-SiA and PDDA-SiA-FTCS membranes was 13.17 LMH, 12.25 LMH and 11.22 LMH, respectively.

Feed and coolant temperatures were 60°C and 20°C, respectively. Feed and coolant flow rates were both maintained at 24 L/h.

The potential behavior of the LBL assembled membranes in AGMD process is schematically depicted in **Fig. 8.** The modification of the PVDF membrane by LBL assembly technique was expected to provide a high surface roughness and fluorinated top layer by SiA and FTCS on to the membrane, leading to the decrease in its surface energy and consequently providing omniphobicity with strong anti-wetting property. Based on the results, for neat PVDF membrane (**Fig. 8** (left figure)), the low surface tension liquids and salt water, like water vapor, can easily penetrate the membrane surface and reach the permeate side. For PDDA-SiA assembled membrane, salt water alone cannot penetrate the SiA layer. However, low surface tension liquids and organic compounds still can pass through the SiA layer and cause membrane wetting, which leads to increase in salt concentration of the permeate water (**Fig. 8** (middle figure)). Although SiA layer contains methyl group which has low surface tension and has higher surface roughness compared with the neat PVDF membrane, it cannot prevent wetting problems against feed solution containing low surface tension liquids and organic compounds. On the other hand, MD process using the PDDA-SiA-FTCS assembled membrane is able to gain a stable normalized water vapor flux and salt rejection performances when treating challenging feed water because of the omniphobic and anti-wetting properties on the membrane surface as contributed by the three-dimensional hierarchical structure (highly rough surface) and fluorinated layer by FTCS (**Fig. 8** (right figure)). Thus, the omniphobic PDDA-SiA-FTCS assembled membrane shows a much higher wetting resistance in MD operation. This clearly shows the potential of the hierarchical omniphobic composite membrane by LBL assembly technique to

510 treat other challenging wastewater containing low surface tension organic contaminants from,
511 textile, food, and oily industries via MD.

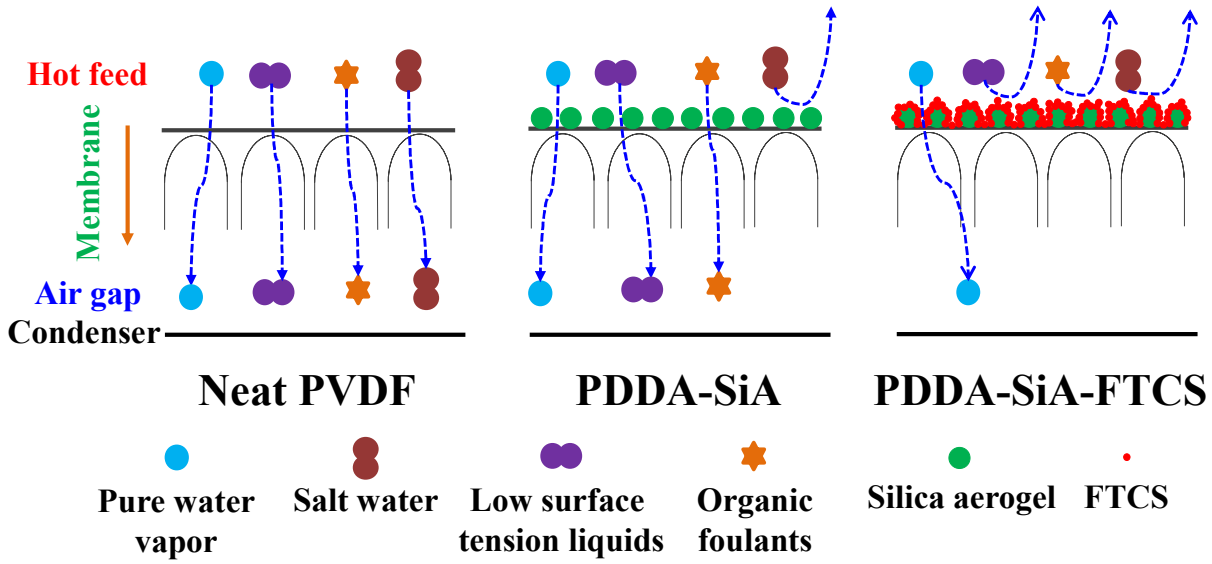

512

513 **Figure 8** Comparison between the behavior of the neat PVDF membrane, PDDA-SiA, and
514 PDDA-SiA-FTCS assembled membranes in AGMD process.

515 In summary, layer-by-layer (LBL) assembly technique was successfully applied on phase
516 inversion poly(vinylidene fluoride) (PVDF) membrane. This study successfully modified the
517 PVDF membrane by LBL assembly technique including fluorination as the formation of
518 trifluoromethyl and tetrafluoroethylene bonds were found to be formed on the membrane surface
519 and high surface roughness were achieved by the formation of hierarchical surface due to silica
520 aerogel (SiA) and 1H, 1H, 2H, 2H – Perfluorodecyltriethoxysilane (FTCS), which led to lower
521 surface free energy and acquirement of omniphobic property on the membrane surface. This
522 could enhance wetting properties of the modified membrane against low surface tension organic
523 contaminants such as methanol, ethylene glycol, and SDS. Although the PDDA-SiA coated
524 membrane showed a high water contact angle (154.14 ± 0.89°), low surface tension organic

contaminants easily passed through the membrane. On the other hand, the PDDA-SiA-FTCS coated membrane had an even higher contact angle of water (177.03 ± 0.41°) and of low surface tension organic liquids (> 162°), which meant that it could be utilized to treat feed containing low surface tension contaminants or organic compounds. Even though the PDDA-SiA-FTCS coated membrane obtained a relatively low water vapor flux (10.55 L/m^{2}h), it gained a much more stable water vapor flux and better salt rejection (~100%) performance than the neat and PDDA-SiA assembled membranes when low concentration of SDS and organic humic acid were added into the real RO brine feed during AGMD operation. The results suggest the high potential of the LBL assembled phase inversion membrane in treatment of challenging feed solutions that may contain organic contaminants such as wastewater from textile, dye, CSG and shale gas produced water in long-term AGMD operation. Future interest in this study may include investigation on effect of the amounts of the LBL layers during modification for treatment of highly saline and organic-rich wastewater.

ASSOCIATED CONTENT

Supporting Information

Supporting – Figure S1. Cross-sectional SEM images of the neat PVDF, PDDA-SiA and PDDA-SiA-FTCS membranes and Video1. LBL WCA Video.avi.

AUTHOR INFORMATION

Corresponding Author

*H. K. Shon, E-mail: Hokyong.Shon-1@uts.edu.au, Tel: +61 2 9514 2629, Fax: +61 2 9514 2633

*L. D. Tijing, E-mail: Leonard.Tijing@uts.edu.au, Tel: +61 9514 2652, Fax: +61 2 9514 2633

Author Contributions

The manuscript was written through contributions of all authors. All authors have given approval to the final version of the manuscript.

Notes

The authors declare no competing financial interest.

ACKNOWLEDGMENT

This research was supported by a grant (17IFIP-B065893-05) from the Industrial Facilities & Infrastructure Research Program funded by Ministry of Land, Infrastructure and Transport of Korean government. The authors also acknowledge the grants from the ARC Future Fellowship (FT140101208) and 2017 FEIT Post Thesis Publication Scholarship by University of Technology Sydney (UTS).

REFERENCES

1. Lee, J.; Boo, C.; Ryu, W. H.; Taylor, A. D.; Elimelech, M., Development of Omniphobic Desalination Membranes Using a Charged Electrospun Nanofiber Scaffold. *ACS Appl Mater Interfaces* **2016,** *8*, (17), 11154-61.

2. Boo, C.; Lee, J.; Elimelech, M., Engineering Surface Energy and Nanostructure of Microporous Films for Expanded Membrane Distillation Applications. *Environ Sci Technol* **2016,** *50*, (15), 8112-8119.

567 3. Lin, S.; Yip, N. Y.; Cath, T. Y.; Osuji, C. O.; Elimelech, M., Hybrid pressure retarded
568 osmosis-membrane distillation system for power generation from low-grade heat:
569 thermodynamic analysis and energy efficiency. *Environ Sci Technol* **2014,** *48*, (9), 5306-13.
570 4. Duong, H. C.; Chivas, A. R.; Nelemans, B.; Duke, M.; Gray, S.; Cath, T. Y.; Nghiem, L.
571 D., Treatment of RO brine from CSG produced water by spiral-wound air gap membrane
572 distillation — A pilot study. *Desalination* **2015,** *366*, 121-129.
573 5. Wang, P.; Chung, T. S., A new-generation asymmetric multi-bore hollow fiber
574 membrane for sustainable water production via vacuum membrane distillation. *Environ Sci*
575 *Technol* **2013,** *47*, (12), 6272-6278.
576 6. Wang, Z.; Hou, D.; Lin, S., Composite Membrane with Underwater-Oleophobic Surface
577 for Anti-Oil-Fouling Membrane Distillation. *Environ Sci Technol* **2016,** *50*, (7), 3866-74.
578 7. Woo, Y. C.; Tijing, L. D.; Shim, W.-G.; Choi, J.-S.; Kim, S.-H.; He, T.; Drioli, E.; Shon,
579 H. K., Water desalination using graphene-enhanced electrospun nanofiber membrane via air gap
580 membrane distillation. *Journal of Membrane Science* **2016,** *520*, 99-110.
581 8. Ge, Q.; Wang, P.; Wan, C.; Chung, T. S., Polyelectrolyte-promoted forward osmosis-
582 membrane distillation (FO-MD) hybrid process for dye wastewater treatment. *Environ Sci*
583 *Technol* **2012,** *46*, (11), 6236-43.
584 9. Nejati, S.; Boo, C.; Osuji, C. O.; Elimelech, M., Engineering flat sheet microporous
585 PVDF films for membrane distillation. *Journal of Membrane Science* **2015,** *492*, 355-363.
586 10. Yang, C.; Li, X.-M.; Gilron, J.; Kong, D.-f.; Yin, Y.; Oren, Y.; Linder, C.; He, T., CF4
587 plasma-modified superhydrophobic PVDF membranes for direct contact membrane distillation.
588 *Journal of Membrane Science* **2014,** *456*, 155-161.

589 11. Prince, J. A.; Singh, G.; Rana, D.; Matsuura, T.; Anbharasi, V.; Shanmugasundaram, T.
590 S., Preparation and characterization of highly hydrophobic poly(vinylidene fluoride) – Clay
591 nanocomposite nanofiber membranes (PVDF–clay NNMs) for desalination using direct contact
592 membrane distillation. *Journal of Membrane Science* **2012,** *397-398*, 80-86.
593 12. Lin, S.; Nejati, S.; Boo, C.; Hu, Y.; Osuji, C. O.; Elimelech, M., Omniphobic Membrane
594 for Robust Membrane Distillation. *Environmental Science & Technology Letters* **2014,** *1*, (11),
595 443-447.
596 13. Woo, Y. C.; Chen, Y.; Tijing, L. D.; Phuntsho, S.; He, T.; Choi, J.-S.; Kim, S.-H.; Shon,
597 H. K., CF4 plasma-modified omniphobic electrospun nanofiber membrane for produced water
598 brine treatment by membrane distillation. *Journal of Membrane Science* **2017,** *529*, 234-242.
599 14. Gogolides, E.; Ellinas, K.; Tserepi, A., Hierarchical micro and nano structured,
600 hydrophilic, superhydrophobic and superoleophobic surfaces incorporated in microfluidics,
601 microarrays and lab on chip microsystems. *Microelectronic Engineering* **2015,** *132*, 135-155.
602 15. Wang, Z.; Elimelech, M.; Lin, S., Environmental Applications of Interfacial Materials
603 with Special Wettability. *Environ Sci Technol* **2016,** *50*, (5), 2132-50.
604 16. Liao, Y.; Loh, C. H.; Wang, R.; Fane, A. G., Electrospun superhydrophobic membranes
605 with unique structures for membrane distillation. *ACS Appl Mater Interfaces* **2014,** *6*, (18),
606 16035-48.
607 17. Liao, Y.; Wang, R.; Fane, A. G., Fabrication of bioinspired composite nanofiber
608 membranes with robust superhydrophobicity for direct contact membrane distillation. *Environ*
609 *Sci Technol* **2014,** *48*, (11), 6335-41.
610 18. Lee, E. J.; Deka, B. J.; Guo, J.; Woo, Y. C.; Shon, H. K.; An, A. K., Engineering the Re-
611 Entrant Hierarchy and Surface Energy of PDMS-PVDF Membrane for Membrane Distillation

612 Using a Facile and Benign Microsphere Coating. *Environ Sci Technol* **2017,** *51*, (17), 10117-
613 10126.
614 19. Hu, M.; Mi, B., Enabling graphene oxide nanosheets as water separation membranes.
615 *Environ Sci Technol* **2013,** *47*, (8), 3715-23.
616 20. Zhao, J.; Pan, F.; Li, P.; Zhao, C.; Jiang, Z.; Zhang, P.; Cao, X., Fabrication of ultrathin
617 membrane via layer-by-layer self-assembly driven by hydrophobic interaction towards high
618 separation performance. *ACS Appl Mater Interfaces* **2013,** *5*, (24), 13275-83.
619 21. Saren, Q.; Qiu, C. Q.; Tang, C. Y., Synthesis and characterization of novel forward
620 osmosis membranes based on layer-by-layer assembly. *Environ Sci Technol* **2011,** *45*, (12),
621 5201-8.
622 22. Brown, P. S.; Bhushan, B., Mechanically durable, superomniphobic coatings prepared by
623 layer-by-layer technique for self-cleaning and anti-smudge. *J Colloid Interface Sci* **2015,** *456*,
624 210-8.
625 23. Hu, M.; Mi, B., Layer-by-layer assembly of graphene oxide membranes via electrostatic
626 interaction. *Journal of Membrane Science* **2014,** *469*, 80-87.
627 24. Woo, Y. C.; Kim, Y.; Shim, W.-G.; Tijing, L. D.; Yao, M.; Nghiem, L. D.; Choi, J.-S.;
628 Kim, S.-H.; Shon, H. K., Graphene/PVDF flat-sheet membrane for the treatment of RO brine
629 from coal seam gas produced water by air gap membrane distillation. *Journal of Membrane*
630 *Science* **2016,** *513*, 74-84.
631 25. Woo, Y. C.; Tijing, L. D.; Park, M. J.; Yao, M.; Choi, J.-S.; Lee, S.; Kim, S.-H.; An, K.-
632 J.; Shon, H. K., Electrospun dual-layer nonwoven membrane for desalination by air gap
633 membrane distillation. *Desalination* **2017,** *403*, 187-198.

634 26. Nghiem, L. D.; Elters, C.; Simon, A.; Tatsuya, T.; Price, W., Coal seam gas produced
635 water treatment by ultrafiltration, reverse osmosis and multi-effect distillation: A pilot study.
636 *Separation and Purification Technology* **2015,** *146*, 94-100.
637 27. Kim, Y.; Lee, S.; Kuk, J.; Hong, S., Surface chemical heterogeneity of polyamide RO
638 membranes: Measurements and implications. *Desalination* **2015,** *367*, 154-160.
639 28. Tang, C. Y.; Kwon, Y.-N.; Leckie, J. O., Characterization of Humic Acid Fouled Reverse
640 Osmosis and Nanofiltration Membranes by Transmission Electron Microscopy and Streaming
641 Potential Measurements. *Environ Sci Technol* **2007,** *41*, 942-949.
642 29. Wang, Y. N.; Tang, C. Y., Nanofiltration membrane fouling by oppositely charged
643 macromolecules: investigation on flux behavior, foulant mass deposition, and solute rejection.
644 *Environ Sci Technol* **2011,** *45*, (20), 8941-7.
645 30. Zuo, G.; Wang, R., Novel membrane surface modification to enhance anti-oil fouling
646 property for membrane distillation application. *Journal of Membrane Science* **2013,** *447*, 26-35.
647 31. Jin, M.; Feng, X.; Xi, J.; Zhai, J.; Cho, K.; Feng, L.; Jiang, L., Super-Hydrophobic PDMS
648 Surface with Ultra-Low Adhesive Force. *Macromolecular Rapid Communications* **2005,** *26*,
649 (22), 1805-1809.
650 32. Artus, G. R. J.; Jung, S.; Zimmermann, J.; Gautschi, H. P.; Marquardt, K.; Seeger, S.,
651 Silicone Nanofilaments and Their Application as Superhydrophobic Coatings. *Advanced*
652 *Materials* **2006,** *18*, (20), 2758-2762.
653 33. Valk, P. v. d.; Pelt, A. W. J. v.; Busscher, H. J.; Jong, H. P. d.; Wildevuur, C. R. H.;
654 Arends, J., Interaction of fibroblasts and polymer surfaces: relationship between surface free
655 energy and fibroblast spreading. *Journal of Biomedical Materials Research* **1983,** *17*, 807-817.

656 34. Liu, G.; Jiang, Z.; Cheng, X.; Chen, C.; Yang, H.; Wu, H.; Pan, F.; Zhang, P.; Cao, X.,
657 Elevating the selectivity of layer-by-layer membranes by in situ bioinspired mineralization.
658 *Journal of Membrane Science* **2016,** *520*, 364-373.
659 35. Amy, G., Fundamental understanding of organic matter fouling of membranes.
660 *Desalination* **2008,** *231*, (1-3), 44-51.
661 36. Hu, M.; Zheng, S.; Mi, B., Organic Fouling of Graphene Oxide Membranes and Its
662 Implications for Membrane Fouling Control in Engineered Osmosis. *Environ Sci Technol* **2016,**
663 *50*, (2), 685-93.
664 37. Wang, M.; Wang, Z.; Wang, X.; Wang, S.; Ding, W.; Gao, C., Layer-by-layer assembly
665 of aquaporin Z-incorporated biomimetic membranes for water purification. *Environ Sci Technol*
666 **2015,** *49*, (6), 3761-8.

667